Myocardial Contrast Echocardiography of Radiofrequency Ablation Lesions

Dorin Panescu*, Liyun Rao, Chuxiong Ding, Huabin Sun, Keith A.Youker, Sherif F. Nagueh and Dirar S. Khoury

From the Center for Experimental Cardiac Electrophysiology, Section of Cardiology, Department of Medicine, Baylor College of Medicine, Houston, Texas, and * EP Technologies/Boston Scientific, San Jose, California, USA

Abstract — ***Introduction:*** **The study tested the feasibility of differentiating radiofrequency ablation lesions from normal myocardium and quantifying their dimensions by myocardial contrast echocardiography (MCE).**
Methods and Results: **In 11 normal dogs, we created 14 focal and 4 linear lesions at different left ventricular sites. MCE was performed both before and after ablation by using an intracardiac echocardiography catheter (9 MHz) and infusing contrast microbubbles through the left coronary artery. An independent observer examined the lesion pathology. We found that intracardiac echocardiography alone could not delineate lesion dimensions. However, after ablation, MCE localized the lesions as well-defined, low-contrast areas within the normally opacified myocardium. Lesion dimensions by MCE immediately after ablation and 30 minutes later were similar. In 12 focal lesions, the average maximum depth (5.55 ± 1.38 mm) and average maximum diameter (10.38 ± 2.09 mm) by MCE were in excellent agreement with the pathologic depth (5.20 ± 1.45 mm) and diameter (10.61 ± 1.67 mm). Two focal lesions could not be detected by MCE and later were found to be superficial. Three-dimensional MCE correctly reconstructed the extent and shape of linear lesions compared to pathology (length: 18.7 ± 5.7 vs 18.5 ± 5.6 mm; maximum longitudinal cross-sectional area: 81.2 ± 9.6 vs 76.0 ± 10.3 mm^2).**
Conclusion: **MCE accurately localized and quantified radiofrequency ablation lesions in the normal left ventricle. This new application of MCE may advance ablation for managing ventricular arrhythmias that involve intramural or epicardial regions by providing instantaneous anatomic feedback on the effects of ablation during catheterization.**

Keywords — **Ablation, Catheter, Echocardiography, Radiofrequency, Ultrasound.**

I. INTRODUCTION

Advancing the management of ventricular tachyarrhythmias by radiofrequency (RF) catheter ablation is contingent on developing techniques that (1) identify the mechanism and location of the arrhythmia with respect to underlying cardiac anatomy and (2) elucidate the effects of ablation therapy. Contrast microbubbles enhance the backscattered ultrasound signal. Consequently, in myocardial contrast echocardiography (MCE), microbubbles have been used during ultrasound imaging to improve the detection of endocardial borders and, more importantly, to assess tissue microvascular perfusion [1]. Intracardiac echocardiography (ICE) has been useful in imaging endocardial structures [2], in guiding RF ablation [3] and in describing tissue characteristics at ablation sites [4]. Our goal was to introduce efficient and clinically applicable means to describe the effects of ablation immediately after delivery of therapy. We assumed that microbubble-rich blood flow in the coronary microcirculation enhance the backscatter of intracardiac ultrasound signals reflected by the normal myocardium, and that blood-deficient ablation lesions subsequently could be distinguished from the neighboring normal myocardium. Our hypothesis was that RF ablation lesions could be differentiated from normal myocardium and quantified by MCE. As a first step towards proving this hypothesis, we examined ablation lesions by contrast-enhanced ICE in the normal heart. While focusing on the normal left ventricle (LV), the present study used contrast enhanced ICE to describe locations and dimensions of ablation lesions, investigate factors impacting their identification, and reconstruct linear ablation lesions.

II. METHODS AND APPARATUS

Eleven mongrel dogs of both sexes (weight 25–35 kg) were included in the study. Once anesthesia was induced with pentobarbital 30 mg/kg, the dogs were endotracheally intubated and ventilated using an external respirator. Continuous intravenous infusion of saline (0.9% sodium chloride) was maintained through the left femoral vein. An intravenous bolus of heparin 100 units/kg was administered. Under the guidance of fluoroscopy, an 8-French coronary lumen catheter (model AL I, Cordis/Johnson & Johnson, Miami, FL) was inserted into the right femoral artery and advanced through the aorta. The catheter tip was placed inside the left main coronary artery and at times was advanced further into either the left anterior descending or the circumflex coronary artery. The catheter provided a means for injecting a suspension of albumin microbubbles (mean diameter range 2.0–4.5 μm, Optison, Amersham Health/GE Healthcare, Princeton, NJ) that created an echogenic contrast effect in the microcirculation. The Optison microbubbles were either infused as a bolus of 0.25 mL followed by a flush of saline injection for imaging focal ablation lesions or administered continuously at a rate of 1 mL/min as a solution of microbubbles mixed in saline (ratio 1:4) for imaging linear ablation lesions. A 10-French soft-tip sheath was inserted into the left femoral artery and advanced through the aorta with the tip placed inside

the LV just below the aortic valve. A 9-French, 9-MHz ICE catheter (model Ultra ICE, EP Technologies/Boston Scientific, San Jose, CA) was inserted through the sheath with the imaging tip positioned inside the LV. The ICE catheter was in turn connected to an imaging console (model ClearView, Scimed/Boston Scientific, San Jose, CA) to acquire echocardiographic images of the LV. To perform 3-D imaging, the ICE catheter was mounted into a pullback device. The pullback device was controlled by a computer-based data acquisition and control system (model Compact 3D IVUS, TomTec Imaging Systems, Unterschleissheim, Germany). The computer system (1) externally controlled the pullback device, (2) acquired continuous ICE images at multiple levels along the LV major axis in 1-mm increments, and (3) reconstructed the LV three-dimensional geometry by stacking multiple ECG- and respiration-gated ICE slices using specialized software (model 4D IVUS Scan Software, TomTec Imaging Systems). Under the guidance of fluoroscopy and ICE, an electrode catheter was inserted into a carotid artery and positioned inside the LV to deliver RF energy. Electrode contact against the LV endocardium was verified by pacing. Focal lesions were created using a 4-mm-tip, 7-French quadripolar electrode catheter (model Blazer II, EP Technologies/Boston Scientific). Linear lesions were created either by dragging an 8-mm-tip, 8-French quadripolar electrode catheter (model Blazer II XP) or using a 9-French loop catheter carrying 14 coil electrodes, each 12 mm long with one or two adjacent electrodes active during RF energy delivery (model Curvilinear Loop, EP Technologies/Boston Scientific). An RF generator (model EPT-1000 or EPT-1000 XP, EP Technologies/Boston Scientific) was used to deliver RF energy between the ablation electrode and an indifferent electrode pad placed on the chest. To produce lesions of diverse size and intramural depth, power-controlled or temperature-controlled RF energy was delivered at different electrode-tissue temperatures (60° – 90°C) and over varying durations (2–5 min). At completion of the study, the dog was sacrificed with KCl, and the heart was excised, opened, and examined. A myocardial block containing the ablation lesion was cut and fixed in 10% buffered formalin. After 24 hours, the ablation lesion was sectioned along the maximum surface diameter by an independent observer, and lesion dimensions were measured. Sections (5-μm thick) were cut and stained with hematoxylin and eosin using standard techniques and examined on a Zeiss Axioscope microscope. The significance of the relationship between MCE measurements and pathologic measurements was assessed by linear regression analysis. Reproducibility of the MCE measurements was quantified by the correlation between the measurements determined at two different time points after ablation. $P < 0.05$ was considered statistically significant.

III. RESULTS

Following intracoronary microbubble infusion, 12 of 14 focal lesions were clearly distinguishable at the ablation electrode locations as well-defined dark spots that lacked contrast enhancement. These spots were not existent in the contrast-enhanced ICE images obtained at baseline. The ablation lesions were well delineated from the surrounding normal myocardium that remained well opacified with microbubbles (Fig. 1). The focal lesions were ellipsoidal in shape, with the maximum diameter below the endocardial surface. These ablation spots were clearly delineated for an average of 10 seconds before the appearance of concentrated intracavitary microbubbles that precluded assessment of the echocardiographic images. The microbubbles were completely washed out of the cavity in about 4 minutes. The remaining 2 of 14 focal lesions could not be visualized following microbubble infusion. Pathologic examination confirmed that those 2 lesions were superficial. No ECG changes were observed with intracoronary microbubble infusion.

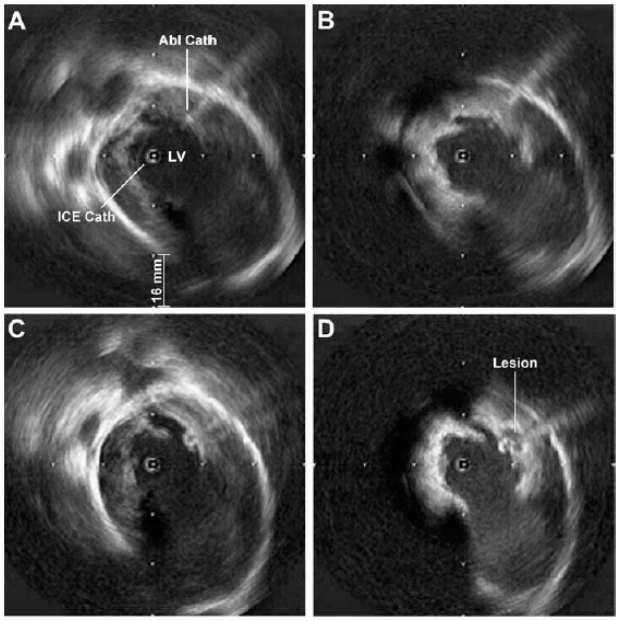

Fig. 1. (A) LV ICE image obtained at baseline. A 4-mm-tip ablation catheter was placed in lateral LV. (B) MCE image obtained at baseline. (C) ICE image obtained after RF energy application in lateral LV. (D) MCE image after RF energy application. A focal lesion was clearly depicted at the site of ablation.

In three extreme cases of charring and coagulum formation during focal ablation, increased echogenicity in the ICE image was evident at the site of ablation after RF energy delivery (Fig. 2A). Even though the

increased echogenicity was indicative of the site of ablation, the ICE image alone could not delineate the intramural depth of the actual lesion. However, intracoronary infusion of contrast microbubbles clearly revealed the extent of the underlying lesion beyond charring, as shown in Fig. 2B, and was confirmed by examining the actual lesion that is shown in Fig. 2C.

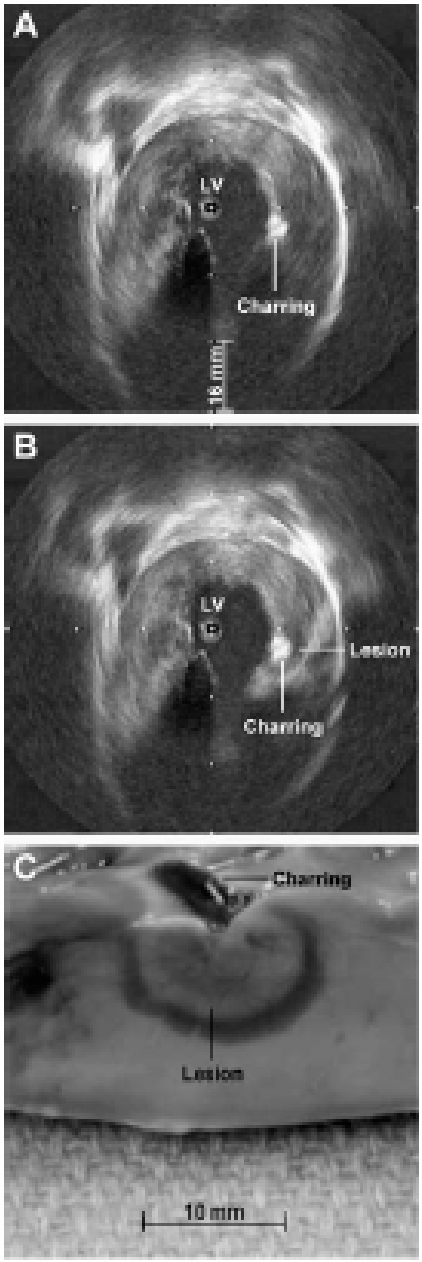

Fig. 2. (A) LV ICE image obtained after ablation. Charring displays increased echogenicity. (B) MCE image of the same lesion. The actual diameter and intramural depth of the lesion were revealed beyond the charring. (C) Cross-section of the corresponding ablation lesion showing the charring on the endocardium.

Ablation lesions were well distinguished and demarcated from adjacent myocardium. Focal lesions were generally ellipsoidal in shape, with the maximum diameter below the endocardial surface. Upon further examination, the ablation lesion consisted of three different regions: (1) central necrosis characterized by loss of nuclei and granulation, (2) tissue hemolysis and capillary injury, and (3) a sharp ring of inflammatory cell infiltration. The peripheral rim had normal myocardium as well as preserved microcirculation and, except for the inflammatory cells, was indistinguishable from the normal myocardium. Accordingly, the peripheral rim was not included in determining the lesion depth and diameter. Lesion maximum depth determined by two-dimensional MCE immediately after ablation was 5.64 ± 1.41 mm, and the maximum depth determined from pathology was 5.20 ± 1.45 mm. The increase in LV local wall thickness due to mural swelling was 1.53 ± 0.71 mm. As illustrated in Fig. 3A, there was an excellent correlation between the maximum depth determined by MCE and the pathologic depth ($r = 0.90$, $n = 12$, $P < 0.001$).

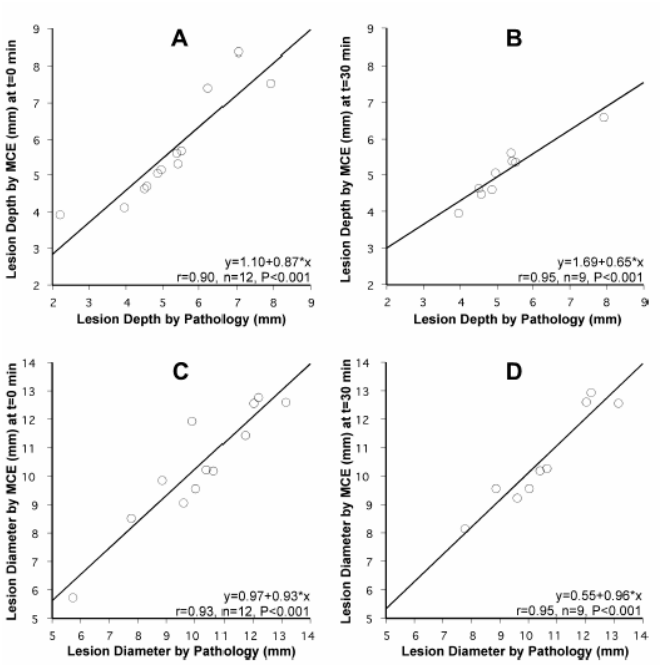

Fig. 3. Focal lesion maximum depth by MCE min vs. the maximum depth by pathologic examination. (A) t=0 min; (B) t=30 min. Focal lesion maximum diameter by MCE vs. the maximum diameter by pathologic examination. (C) t=0 min; (D) t=30 min.

Lesion maximum depth determined by MCE 30 minutes after RF energy delivery was 5.09 ± 0.77 mm and had an excellent correlation with the pathologic depth ($r = 0.95$, $n = 9$, $P < 0.001$; Fig. 3B). Reproducibility of the MCE lesion depth was confirmed by the high correlation between both time points ($r = 0.99$, $P <$

0.001). The difference in lesion depth at the two time points was 0.25 ± 0.29 mm. Lesion maximum diameter determined by two dimensional MCE immediately after ablation was 10.39 ± 2.07 mm, and the maximum diameter determined from pathology was 10.14 ± 2.06 mm. As illustrated in Fig. 3C, there was an excellent correlation between the maximum diameter determined by MCE and the pathologic diameter ($r = 0.93$, $n = 12$, $P < 0.001$). Lesion maximum diameter determined by MCE 30 minutes after RF energy delivery was 10.59 ± 1.72 mm and had an excellent correlation with the pathologic diameter ($r = 0.95$, $n = 9$, $P < 0.001$; Fig. 3D). Reproducibility of the MCE lesion diameter was confirmed by the high correlation between both time points ($r = 0.99$, $P < 0.001$). The difference in lesion diameter at the two time points was 0.14 ± 0.13 mm.

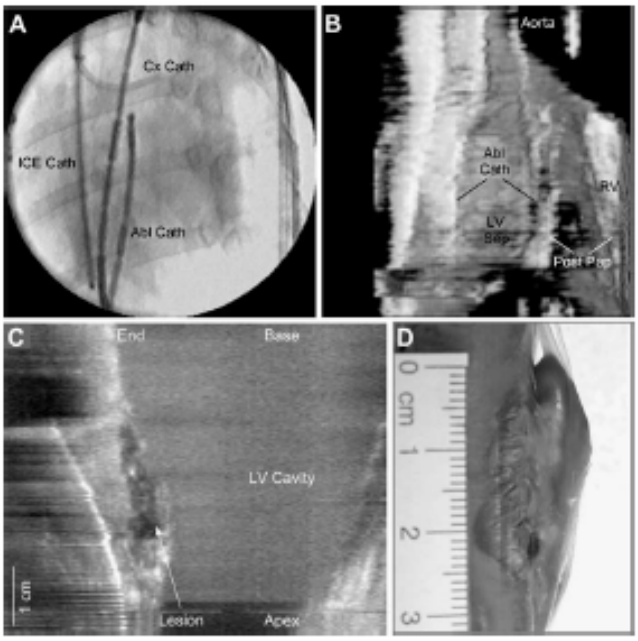

Fig. 4. (A) Radiograph depicting a 14-electrode ablation catheter and an ICE catheter inside a sheath in the LV. A lumen catheter is placed in the circumflex coronary artery. (B) 3-D ICE reconstruction of the LV interior depicting the ablation catheter and anatomic features such as the LV septum and posterior papillary muscle. (C) 3-D MCE reconstruction of the LV depicting a linear lesion created by two adjacent electrodes in posterior region. (D) Corresponding longitudinal sectional view of the ablation lesion.

A radiographic image of a loop ablation catheter inside the LV is depicted in Fig. 4A, and corresponding geometry reconstructed by three-dimensional echocardiography is shown in Fig. 4B. A lesion was created in posterior LV by two adjacent electrodes on the loop catheter and was successfully reconstructed by three-dimensional MCE (Fig. 4C) as compared to pathology (Fig. 4D). Linear lesion maximum length determined by three-dimensional MCE immediately after ablation was 18.7 ± 5.7 mm, and maximum length determined from pathology was 18.5 ± 5.6mm ($r=0.99$, $n=4$, $P < 0.001$). Meanwhile, linear lesion maximum longitudinal cross-sectional area (from endocardium to epicardium) was 81.2 ± 9.6 mm^2 by MCE and 76.0 ± 10.3 mm^2 by pathology ($r = 0.91$, $n = 4$, $P < 0.001$). Lesions produced with the 8-mm tip were also successfully reconstructed.

IV. CONCLUSIONS

The present study describes the first application of two-dimensional contrast-enhanced ICE in localizing RF ablation lesions and accurate quantification of their extent and depth within the myocardium in the intact beating heart. Furthermore, the study extends this application and presents, for the first time, a novel method based on contrast-enhanced three-dimensional ICE to describe details of contiguous linear lesions. Intracoronary infusion of Optison microbubbles during ICE imaging clearly distinguished acute RF ablation lesions. The lesions appeared as dark, low-contrast spots that were distinct from the adjacent normally opacified myocardium. The lesions identified by MCE were always consistent with the locations of the ablation electrode and had topography similar to that observed on pathologic examination. The MCE lesion dimensions were in excellent agreement with the corresponding pathologic dimensions. This new application of MCE may advance ablation for management of ventricular arrhythmias that involve intramural or epicardial regions by providing anatomic feedback on the effects of ablation during catheterization.

V. REFERENCES

[1] A. J. Kemper, T. Force, L. Perkins, M. Gilfoil and A. F. Parisi, "In vivo prediction of the transmural extent of experimental acute myocardial infarction using contrast echocardiography," *J Am Coll Cardiol* vol. 8, pp. 143-149, 1986.

[2] J. F. Ren, D. Schwartzman, D. J. Callans, S. E. Brode, C. D. Gottlib and F. E. Marchlinski, "Intracardiac echocardiography (9 MHz) in humans: Methods, imaging views and clinical utility," *Ultrasound Med Biol* vol. 25, pp. 1077-1086, 1999.

[3] F. X. Roithinger, P. R. Steiner, Y. Goseki, K. S. Liese, D. B. Scholtz, A. Sippensgroenewegen, P. Ursell and M. D. Lesh, "Low-power radiofrequency application and intracardiac echocardiography for creation of continuous left atrial linear lesions," *J Cardiovasc Electrophysiol* vol. 10, pp. 680-691, 1999.

[4] J. F. Ren, D. J. Callans, D. Schwartzman, J. J. Michele and F. E. Marchlinski, "Changes in local wall thickness correlate with pathologic lesion size following radiofrequency catheter ablation: An ICE imaging study," *Echocardiography* vol. 18, pp. 503-507, 2001.